A study on the medium range order in molten Fe_3Si and FeSi alloys

2004 J. Phys.: Condens. Matter 16 4753

(http://iopscience.iop.org/0953-8984/16/28/001)

INSTITUTE OF PHYSICS PUBLISHING JOURNAL OF PHYSICS: CONDENSED MATTER

J. Phys.: Condens. Matter **16** (2004) 4753–4760 PII: S0953-8984(04)76329-8

A study on the medium range order in molten Fe_3Si and FeSi alloys

Jingyu Qin, Tingkun Gu and Xiufang Bian

Key Laboratory of Liquid Structure and Heredity of Materials, Shandong University, No. 73 Jingshi Road, 250061, Jinan, People's Republic of China

E-mail: qinjy@sdu.edu.cn

Received 17 February 2004
Published 2 July 2004
Online at stacks.iop.org/JPhysCM/16/4753
doi:10.1088/0953-8984/16/28/001

Abstract

Prepeaks are observed in the x-ray diffraction patterns of molten Fe_3Si and FeSi alloys and the mechanism of their microstructures is discussed. The distance in real space corresponding to the prepeak positions resembles that of the Si–Si distances in the $D0_3$ type crystal of Fe_3Si within a deviation of 2.4%. Furthermore, by the reverse Monte Carlo (RMC) simulation, the prepeak is only found in the partial structure $S_{SiSi}(Q)$ for molten Fe_3Si alloy, while in molten FeSi alloy prepeaks are found in both $S_{SiSi}(Q)$ and $S_{FeFe}(Q)$ with similar height. The Gaussian distribution is found in the partial coordination number distribution of Fe atoms around a Si atom in the two alloys. The dominant 7-coordination in molten FeSi alloy suggests that Fe_7Si and $FeSi_7$ type clusters are kept in the molten state from FeSi crystal. Si–Si coherent packing should be responsible for the medium range order (MRO) of molten Fe_3Si while Fe–Fe and Si–Si coherent packing for that of molten FeSi.

1. Introduction

The binary Fe–Si phase diagram [1] shows it is a complex system with several intermetallic compounds such as Fe_3Si, Fe_2Si, FeSi, Fe_2Si_5 and $FeSi_2$, etc. Many of them are of high industrial interest. The $D0_3$ type Fe_3Si is one kind of magnetic material [2]. The ε-FeSi alloy that belongs to magnetic semiconductors [3] is stable at ambient temperature and has a melting temperature as high as 1410 °C. The compounds Fe_2Si_5 and $FeSi_2$ alloys are newly found good thermoelectric materials [4].

It is pointed out [5, 6] that the molten structure of Fe–Si alloys and pure Si can affect the performance and quality of the crystals manufactured from their melts. Since there is an intrinsic relation between the structure, density, viscosity and surface tension in the molten state, the study on the molten structure of Fe–Si alloys is then valuable to improve manufacturing technology and to reveal the complex interaction nature between Fe and Si in condensed matter.

By means of a quasi-eutectic alloy model, Vatolin *et al* [7] analysed the x-ray diffraction results of molten Fe_3Si, FeSi and $FeSi_2$ alloy. In the systematic study on Fe–Si alloy system carried out by Kita *et al* [8], it was concluded that the structure of the Fe–Si alloys with Si content less than 40% could be described by a hard sphere model. However all prepeaks are neglected. Sedelmeyer *et al* [9] found that a satisfactory result could be reached in describing the liquid structure of $FeSi_2$ and Fe_2Si based on a crystal-like structure model. Recently, Il'inskii *et al* [10] proposed an inhomogeneous structure model for the molten Fe–Si alloys.

The prepeaks in the structure factors of molten Fe_3Si and FeSi seem to be abnormal. Particular attention needs therefore to be paid to the origin of the prepeaks in molten Fe_3Si and FeSi alloys. To do this, we employed the reverse Monte Carlo (RMC) simulation for investigating the correlation between the structure of the solid and the liquid state.

2. Experimental details

Pure Fe (99.98%) and pure Si (99.999%) were melted at 1650 °C under an atmosphere of He of high purity. Then the alloy melts were cooled down and kept at 1550 °C for 2 h before x-ray diffraction experiments were executed. The mass densities of the two alloy melts at 1550 °C were 5.58 and 4.36 g cm^{-3} that were interpolated from the data reported in [11, 12], with the number density being 0.073×10^3 and 0.069×10^3 nm^{-3}, respectively.

The x-ray diffraction intensity was collected and converted to the structure factor $S(Q)$ after a correction and normalization procedure that was described in detail in [13]. The structure factor $S(Q)$ related to the pair correlation function $g(r)$ is defined by equation (1):

$$g(r) = 1 + \frac{c_1 f_1^2 + c_2 f_2^2}{2\pi^2 r \rho_0 (c_1 f_1 + c_2 f_2)^2} \int_0^\infty [S_{\mathrm{AL}}(Q) - 1] Q \sin(Qr)\, \mathrm{d}Q \tag{1}$$

where the subscript AL on $S(Q)$ means the Ashcroft–Langreth structure factor, the numbers 1 and 2 represent the Fe or Si atom type the variables c and f denote the concentration and the atomic scattering factor of an alloy element and ρ_0 is the number density of the alloy at 1550 °C.

The total coordination number can be evaluated by equation (2):

$$N_{\min} = \int_{r_0}^{r_{\min}} 4\pi r^2 \rho_0 g(r)\, \mathrm{d}r \tag{2}$$

where the lower integration limit r_0 and the upper limit $r_{\min}$ define the borders of the first peak of the integration function.

An alternative method used in this article is the RMC simulation [14, 15] that is now widely employed to model the structure of crystalline and non-crystalline materials. The parameters such as the alloy concentration, the density and the minimum and maximum atomic distances are essential for the RMC simulation. It is better to use coordination as additional constraints if possible. In this work 4000 atoms were used in the RMC simulation that started from a random configuration. The simulation boxes are cubic with the length of 3.78 nm for Fe_3Si and 3.87 nm for FeSi being sufficient for the study of MRO.

It is believed that a prepeak in the $S(Q)$ of the melt means a close correlation between the crystalline and the molten structures. Therefore partial coordination constraints could be applied to the RMC simulation according to the characteristics of the crystal structure. Specifically the constraints are so designed that from r_0 to $r_{\min}$ there are 10 and 7 Fe atoms surrounding a Si atom for Fe_3Si and FeSi respectively. As in equation (2), the values of r_0 and $r_{\min}$ are 0.20 and 0.34 nm, respectively.

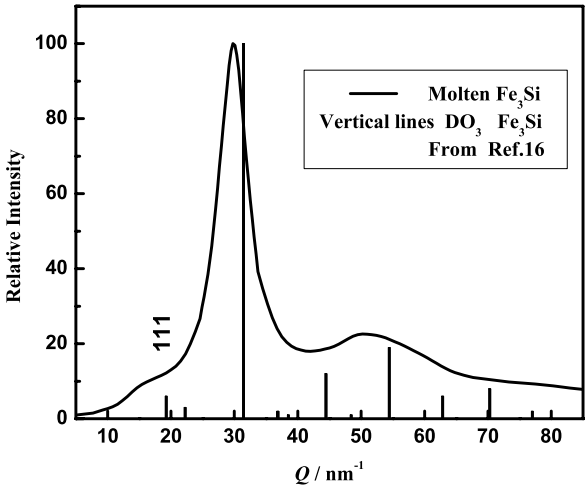

Figure 1. X-ray diffraction intensity of molten Fe_3Si.

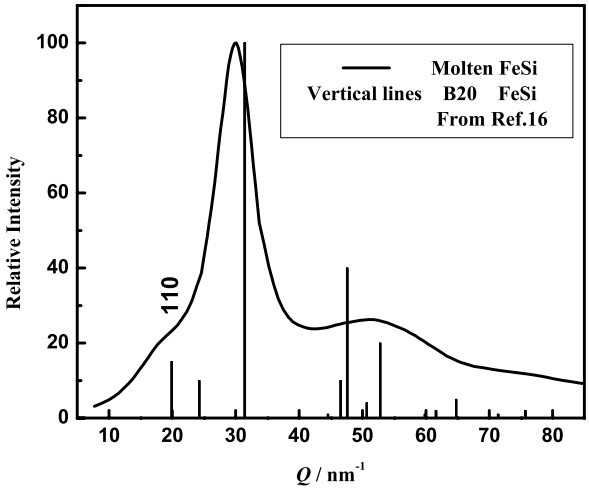

Figure 2. X-ray diffraction intensity of molten FeSi.

3. Results and discussion

The x-ray diffraction intensity curves of molten Fe_3Si and FeSi alloys are illustrated in figures 1 and 2, respectively, with the maximum intensity scaled to 100 in order to be compared with the crystalline powder diffraction pattern [16]. Prepeaks in the intensity curves imply that the MRO exists in the melts studied. Following Qin *et al* [13], the prepeak positions were determined as 16 and 18 nm^{-1} for molten Fe_3Si and FeSi alloys, respectively. As far as the intensity at the position of prepeak is concerned, molten Fe_3Si alloy is weaker than molten FeSi alloy. It suggests that the MRO in molten Fe_3Si alloy is weaker than that in molten FeSi alloy. Moreover, the diffraction pattern of the superstructures of $D0_3$ type Fe_3Si and B20 type FeSi alloys can be found near the prepeaks. As shown in figures 1 and 2, the first reflections from the left are indexed as 111 for the $D0_3$ type Fe_3Si alloy and 110 for the B20 type FeSi alloy. The former is observably weaker than the latter. The prepeak and the superstructure diffraction

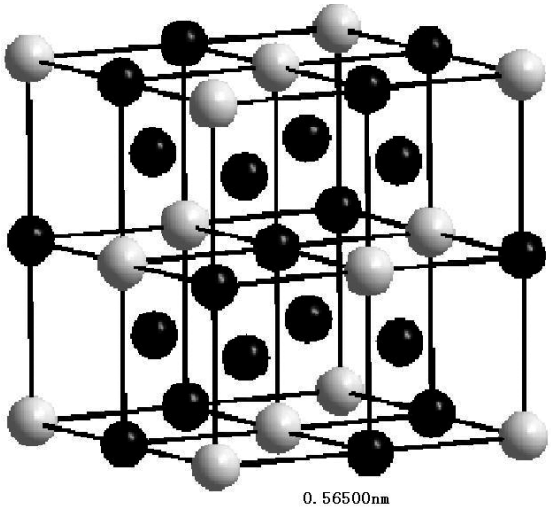

Figure 3. Crystal unit cell of $D0_3$ type Fe_3Si alloy (black ball: Fe atom, white ball: Si atom, crystal lattice parameter: 0.565 00 nm).

Table 1. Characteristic position of x-ray diffraction patterns of Fe_3Si and FeSi alloys.

Alloy	Q_{pre} (nm^{-1})	Q_{super} (nm^{-1})	Q_{main} (nm^{-1})	Q_{max} (nm^{-1})
Fe_3Si	16	19.2	29.8	31.4
FeSi	18	19.8	29.9	31.4

pattern are homologous. The stronger superstructure diffraction pattern is accompanied with the stronger prepeak.

In table 1, Q_{pre} and Q_{main} denote the positions of the prepeak and the first peak in the molten intensity curves, respectively; Q_{super} and Q_{max} indicate the first reflection from the left and the line with the maximum intensity in the powder diffraction pattern, respectively.

For molten Fe_3Si alloy, Q_{pre} is 17% less than Q_{super} while Q_{main} is only 5% less than Q_{max}. It follows that variation of atomic packing takes place mainly in the MRO range rather than in the SRO range.

The crystal unit cell of $D0_3$ type Fe_3Si alloy [17] is illustrated in figure 3. Each Si atom has eight Fe atoms coordinated at 0.2447 nm, with no Si atom being the nearest neighbour. The measure of the third coordination shell lies about 0.3995 nm and each Si atom is surrounded by eight Fe atoms or slightly more. These features may be kept in the molten state during the melting process. By the quasi-Bragg equation $d = 2\pi/Q_{pre}$, the distance in real space corresponding to $Q_{pre} = 16\,nm^{-1}$ is 0.39 nm, which is rather close to the nearest Si–Si distance in $D0_3$ type Fe_3Si, with a deviation of only 2.4%. This suggests that most Fe atoms surround Si atoms to form Si-centred clusters, with the favourite Si–Si distance being about 0.39 nm among such clusters.

The transformation from the Bragg peak 111 to prepeak can be explained as follows. The reflection 111 is so weak that the corresponding crystal plane can easily be distorted by thermal excitation. However, the packing of Si atoms in the melt is not all at random, the coherent packing of the Si-centred clusters results in the prepeak in $S(Q)$ of molten Fe_3Si.

As to molten FeSi, the change of Q_{main} with Q_{max} is similar to that of molten Fe_3Si, as shown in table 1. The difference between Q_{pre} and Q_{super} is only 9.1%. It is significantly less

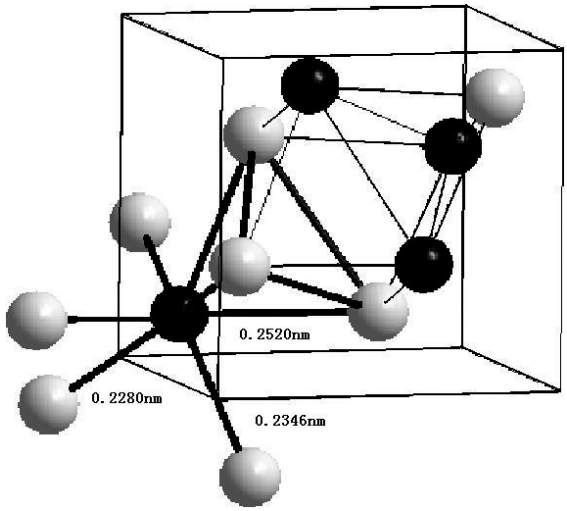

Figure 4. Crystal unit cell of B20 type FeSi alloy and one of its Si_7Fe cluster (black ball: Fe atom, white ball: Si atom, crystal lattice parameter: 0.449 50 nm).

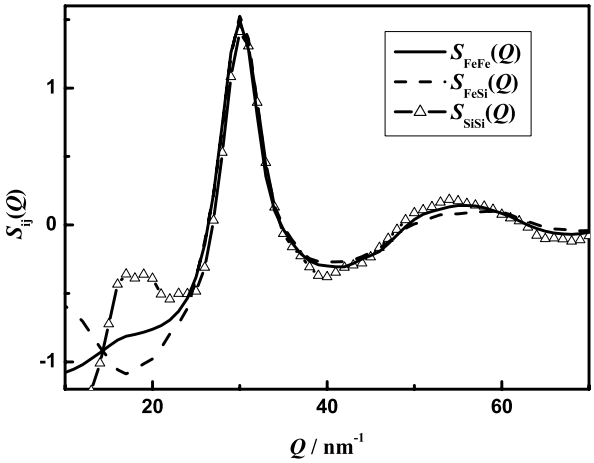

Figure 5. Partial structure factors from RMC simulation on molten Fe_3Si alloy.

than that of molten Fe_3Si. The correlation between the crystalline and the molten structure in FeSi alloy is then stronger than that in Fe_3Si alloy.

The atom coordination in B20 type FeSi alloy is more complicated than that in $D0_3$ type Fe_3Si alloy. The B20 crystal unit cell of FeSi alloy [18] and one of its $FeSi_7$ clusters which are equivalent to Fe_7Si clusters are shown in figure 4. In B20 type FeSi alloy, Fe and Si atoms are equivalent and each atom is surrounded with seven unlike atoms within 0.275 nm. Since the atom packing is so complicated, it is difficult to relate the prepeak position with a characteristic distance in real space by quasi-Bragg equation.

To exploit further details of the MRO in molten Fe_3Si and FeSi alloys based on the above analysis, RMC simulations were carried out on molten Fe_3Si and FeSi alloys with partial coordination constraints on Si. As shown in figure 5, there is a prepeak in the partial structure

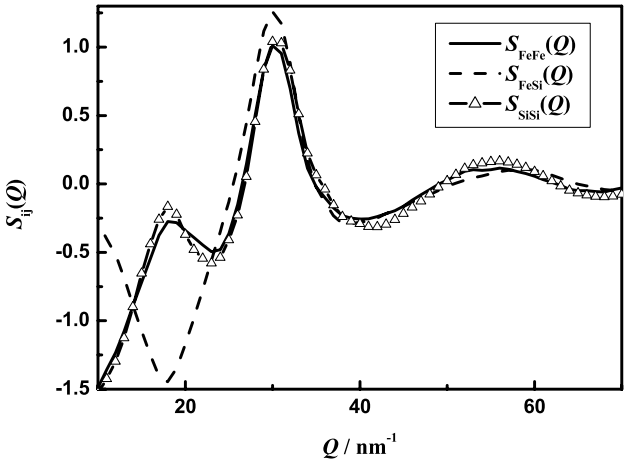

Figure 6. Partial structure factors from RMC simulation on molten FeSi alloy.

factor $S_{SiSi}(Q)$ and a valley in $S_{FeSi}(Q)$ at approximately the same position. It should be noted that in the range 10–20 nm^{-1}, the shape of $S_{FeFe}(Q)$ resembles that of the total structure factor $S(Q)$ of molten Fe_3Si. This may be caused by the RMC method itself since the RMC simulation on molten Fe_3Si without coordination constraints always yields to this kind of $S_{FeFe}(Q)$. By the RMC simulation it is proved that the prepeak in the $S(Q)$ of Fe_3Si melt originates from the prepeak in $S_{SiSi}(Q)$. It is then speculated that the MRO is determined by the packing of Si-centred clusters, or in other words, rather than the nearest coordination of Si atoms.

As plotted in figure 6, at 18 nm^{-1} the $S_{FeSi}(Q)$ in molten FeSi alloy has a valley which indicates the priority of coordination of unlike atoms over like atoms. However the presence of prepeaks in both the $S_{FeFe}(Q)$ and the $S_{SiSi}(Q)$ at 18 nm^{-1} implies that the MRO structure in molten FeSi alloy should be attributed to the coherent packing of both Fe–Fe and Si–Si, and that Fe atoms possess the similar environment to Si atoms.

We select partial pair correlation functions of the $g_{SiSi}(r)$ for Fe_3Si and the $g_{FeSi}(r)$ for FeSi to illustrate the local structural relationship between the crystal and the melt, as shown in figure 7, where the maximum height of the $g_{SiSi}(r)$ and the $g_{FeSi}(r)$ are scaled to 2 for convenience. Under the first peak of the $g_{FeSi}(r)$, three vertical lines of B20 FeSi alloy with the total coordination number of 7 are found. This suggests that the coordination of unlike atoms in molten FeSi alloy is similar to that in the B20 FeSi crystal. However, the Si–Si coordination in $D0_3$ Fe_3Si changes evidently after melting. As described in the preceding paragraph, there are no Si atoms less than 0.3995 nm in $D0_3$ Fe_3Si crystal, whereas in molten Fe_3Si the first coordination shell is located at 0.25 nm, with the second peak at 0.45 nm. Nevertheless, the position of the Si–Si coordination line for $D0_3$ Fe_3Si still overlaps the second peak of $g_{SiSi}(r)$ for molten Fe_3Si. Furthermore, we pay attention to height ratio of the second peak to the first peak in the partial pair correlation functions for molten Fe_3Si, and the calculated values are 0.61, 0.54 and 0.64 for the $g_{FeFe}(r)$, the $g_{FeSi}(r)$ and the $g_{SiSi}(r)$, respectively. Therefore the second peak of $g_{SiSi}(r)$ has the maximum height and that of $g_{FeSi}(r)$ has the minimum height relative to their first peaks. This means that in molten Fe_3Si the tendency of no Si–Si coordination as the nearest neighbour was kept from the crystalline state to some extent.

Additional information can be driven from the distribution of the partial coordination number N_{SiFe}, i.e. the Fe atoms surrounding a Si atom in molten Fe_3Si and FeSi alloys. As

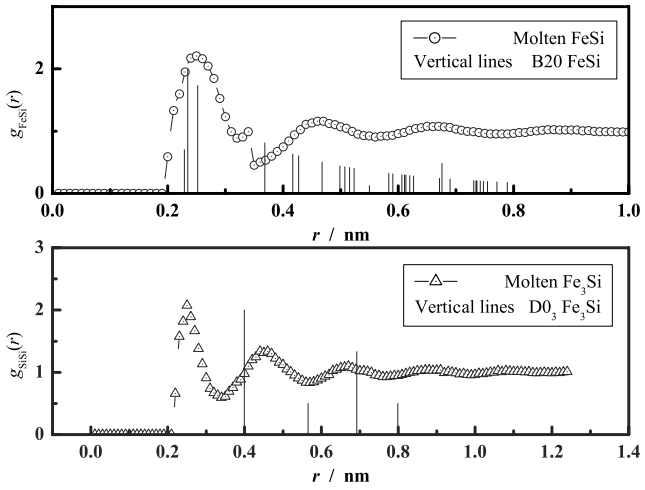

Figure 7. Selected partial pair correlation functions for Fe_3Si and FeSi alloy.

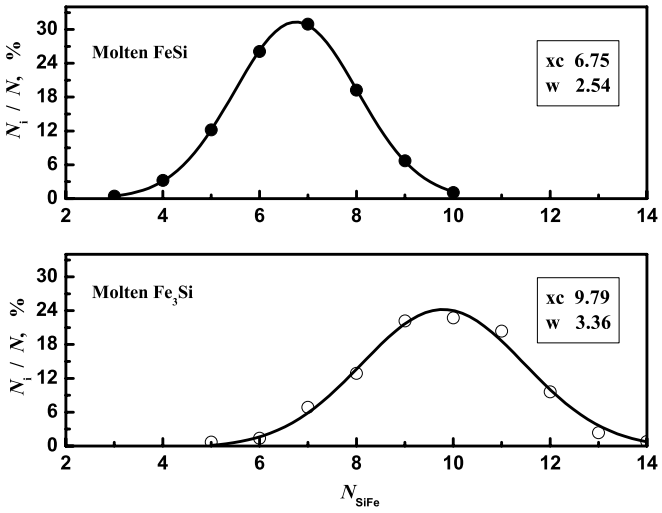

Figure 8. Distribution of the partial coordination number N_{SiFe} in molten Fe_3Si and FeSi alloys (xc: centre of the Gaussian distribution; w: width of the Gaussian distribution).

shown in figure 8, the data can be well fitted by a Gaussian distribution with a centre of 9.79 and width of 3.53 for molten Fe_3Si, and 6.75 and 2.54 for molten FeSi. From the cluster point of view, the wider distribution of N_{SiFe} in molten Fe_3Si corresponds to more kinds of Si-centred clusters so that the topological packing of these clusters may be more distorted and as a result the MRO becomes weaker.

In contrast, the distribution curve of N_{SiFe} in molten FeSi is narrower and sharper. The 7-coordination reaches a portion of approximately one-third. It is proved that in molten FeSi alloy, the Fe_7Si- or $FeSi_7$-like clusters are inherited out of B20 type crystal. The prepeak in the $S(Q)$ curve of molten FeSi alloy is stronger than that of molten Fe_3Si and its position comes close to the line indexed with 110.

The above structural characteristics in molten Fe_3Si and FeSi alloys are thought to originate from the strong interaction between Fe and Si atoms. Using high-resolution Si Kα x-ray

fluorescence spectra Liu *et al* [19] measured the effective charge on each Si atom in $FeSi_2$, FeSi and Si steel, which is +0.56 electrons per Si atom in FeSi alloy. It is then easy to calculate by interpolation that in Fe_3Si alloy each Si atom has an effective charge of +0.61 electrons which is very close to +0.62 electrons per atom of Si in SiO_2. This is the experimental evidence of strong interaction between Fe and Si atoms in Fe_3Si and FeSi alloys. Since the effective charge of an element is determined mainly by the electronegativity of the other element interacting with it and less by its coordination number, the result could be applied to understand the atomic interaction in molten Fe_3Si and FeSi alloys. It is then reasonable that Fe atoms would prefer to have Si atoms rather than Fe atoms as nearest neighbours and vice versa. In the case of FeSi, the local structural characteristic of 7-coordination clusters in the B20 alloy will preserve the melt to a large extent. For Fe_3Si alloy, since Si is a minor species, they prefer to be surrounded by Fe atoms so that weak MRO forms in the melt.

4. Conclusions

MRO in molten Fe_3Si and FeSi alloy is observed by x-ray diffraction experiments and analysed by reverse Monte Carlo. In molten Fe_3Si, the MRO originates from the coherent packing of Si-centred clusters, while in molten FeSi the coherent packing of both kinds of Fe- and Si-centred clusters contribute much to the MRO. The most favoured Si–Si distance in molten Fe_3Si is 0.405 nm, that is nearly the same as the Si–Si distance in $D0_3$ type crystal. Fe_7Si- and $FeSi_7$-like clusters will be kept in the melt as the B20 type FeSi alloy is melted.

Acknowledgments

The authors would like to thank Professor W M Wang and Dr J X Zhang for reading the script. This work is partially supported by the NSFC under the contract no. 50231040

References

[1] Massalski T B (ed) 1986 *Binary Alloy Phase Diagram* (Metals Park, OH: ASM International) p 1108
[2] Kudrnovský J, Christensen N E and Andersen O K 1991 *Phys. Rev.* B **43** 5924
[3] Corti M, Aldrovandi S, Fanciulli M and Tabak F 2003 *Phys. Rev.* B **67** 172408
[4] Yamauchi I, Okamoto T, Ohata H and Ohnaka I 1997 *J. Alloys Compounds* **260** 162
[5] Kita Y, Van Zytveld J B, Morita Z and Iida T 1994 *J. Phys.: Condens. Matter* **6** 811
[6] Waseda Y, Shinoda K, Sugiyama K, Takeda S, Terashima K and Toguri J M 1995 *Japan. J. Appl. Phys.* 1 **34** 4124
[7] Vatolin N A and Pashtuhov E A 1980 *Diffraction Study on the Structure of High Temperature Melts* (Moscow: Science Press) chapter 2 (in Russian)
[8] Kita Y, Zeze M and Morita Z 1982 *Trans. ISIJ* **22** 571
[9] Sedelmeyer B and Steeb S 1997 *Z. Naturf.* a **52** 415
[10] Il'inskii A, Slyusarenko S, Slukhovskii O, Kaban I and Hoyer W 2002 *J. Non-Cryst. Solids* **306** 90
[11] Dumay C and Cramb A V 1995 *Metall. Mater. Trans.* B **26** 173
[12] Andronov V N, Qiekin B V and Nesterenko S V 1977 *Liquid Metals and Slags* (Moscow: Metal Physics) p 10 (in Russian)
[13] Qin J Y, Bian X F, Sliusarenko S I and Wang W M 1998 *J. Phys.: Condens. Matter* **10** 1211
[14] McGreevy R L and Pusztai L 1988 *Mol. Simul.* **1** 359
[15] McGreevy R L 2001 *J. Phys.: Condens. Matter* **13** R877
[16] 1998 JCPDS International Centre for Diffraction Data, PDF-2 Data Base (Sets 1–48 plus 70–85) Fe_3Si: 45–1207, FeSi: 78-1748
[17] Mishra S N, Rambabu D, Grover A K, Pillay R G, Tandon P N, Devare H G and Vijayaraghavan R 1985 *J. Appl. Phys.* **57** 3258
[18] Wartchow R, Gerighausen S and Binnewies M 1997 *Z. Kristallogr.-New Cryst. Struct.* **212** 320
[19] Liu Z L, Sugata S, Yuge K, Nagasono M, Tanaka K and Kawai J 2004 *Phys. Rev.* B **69** 035106